How to cite: *Angew. Chem. Int. Ed.* **2022,** *61,* e202213495
International Edition: doi.org/10.1002/anie.202213495
German Edition: doi.org/10.1002/ange.202213495

VIP **Bioimaging** *Very Important Paper*

In Vivo Nitroreductase Imaging via Fluorescence and Chemical Shift Dependent ^{19}F NMR

*Shizhen Chen[+], Long Xiao[+], Yu Li, Maosong Qiu, Yaping Yuan, Rui Zhou, Conggang Li, Lei Zhang, Zhong-Xing Jiang, Maili Liu, and Xin Zhou**

Abstract: Nitroreductase (NTR) is an important biomarker widely used to evaluate the degree of tumor hypoxia. Although a few optical methods have been reported for detecting nitroreductase at low concentration ranges, an effective strategy for nitroreductase monitoring in vivo without limits to the imaging depth is still lacking. Herein, a novel dual-mode NIR fluorescence and ^{19}F MRI agent, FCy7-NO_2, is proposed for imaging tumor hypoxia. We show that FCy7-NO_2 serves as not only a rapid NIR fluorescence enhanced probe for monitoring and bioimaging of nitroreductase in tumors, but also a novel ^{19}F MR chemical shift-sensitive contrast agent for selectively detecting nitroreductase catalyzed reduction. Notably, integrating two complementary imaging technologies into FCy7-NO_2 enables sensitive detection of nitroreductase in a broad concentration range without tissue-depth limit. In general, this agent has a remarkable response to nitroreductase, which provides a promising method for understanding tumor evolution and its physiological role in the hypoxic microenvironment.

Introduction

Lung cancer remains the most common cancer worldwide and the leading cause of death from malignant tumors.[1] Early detection and diagnosis of lung cancer is the key to reducing mortality. Low-dose computed tomography (CT) has been widely used for early lung cancer screening since 2011. However, apart from the risk of radiation exposure, it suffers low specificity and a high rate of false positives.[2] Magnetic resonance imaging (MRI) can generate images of higher temporal and spatial resolution without ionizing radiation. Conventional proton (^{1}H) MRI is routinely used due to the unparalleled contrast to depict anatomical structure in soft tissues.[3] However, ^{1}H MRI suffers very low sensitivity in the lungs because of the cavity structure without abundant endogenous protons.[4] In contrast, ^{19}F nuclei are attractive for imaging due to 100% natural abundance, no background interference, broad chemical shift range (>350 ppm) and high gyromagnetic ratio (40.06 MHz T^{-1}).[5] ^{19}F MRI with exogenous contrast agents looks promising for "hot-spot" lung imaging and spectroscopy.

In solid tumors, uncontrolled cell growth leads to the depletion of oxygen within the cytoplasm of cells at a rate that far exceeds the rate of replenishment from the blood supply. The concentration of oxygen in hypoxic cells can vary from 0.02 to 2% (below 2.5 mmHg pO_2), while in normoxic cells it can range from 2 to 9% (40 mmHg pO_2).[6] Clinical research has indicated that oxygen starvation of tumors is closely related to tumor progression toward a more malignant phenotype with increased metastatic potential.[7] Moreover, tumor hypoxia usually leads to therapeutical resistance to chemotherapy and radiotherapy.[8] Therefore, estimating the degree of hypoxia is significant for early detection and effective intervention of tumors. Notably, hypoxia is generally accompanied by elevated reductive enzymes, such as nitroreductase, DT-diaphorase, and azoreductase.[9] Among them, nitroreductase concentration has been considered directly related to the degree of hypoxia.[10] Thus, the detection of the nitroreductase levels can be used to probe the degree of hypoxia in a tumor.

Nitroreductase, a cytosolic enzyme, can use beta-Nicotinamide adenine dinucleotide (NADH) as an electron source to reduce the nitro groups to the corresponding amines.[11] The significant electronic change resulting from the conversion of the electron-withdrawing nitro group to the electron-donating amino group provides a selective "switch" mechanism for activating an inert compound, which leads to the subsequent release of the active agent. Based on the switch mechanism, various activatable imaging probes have been designed with nitro compounds as substrates to be triggered upon reduction by nitroreductase. For example, Li and co-workers[12] have synthesized five near-infrared (NIR) cyanine dyes with fluorescence reporting structures decorated with different nitroaromatic groups. The experimental

[*] Dr. S. Chen,[+] L. Xiao,[+] Dr. Y. Li, M. Qiu, Dr. Y. Yuan, Dr. R. Zhou, Prof. Dr. C. Li, Dr. L. Zhang, Prof. Dr. Z.-X. Jiang, Prof. Dr. M. Liu, Prof. Dr. X. Zhou
State Key Laboratory of Magnetic Resonance and Atomic and Molecular Physics, National Center for Magnetic Resonance in Wuhan, Wuhan Institute of Physics and Mathematics, Innovation Academy for Precision Measurement Science and Technology, Chinese Academy of Sciences—Wuhan National Laboratory for Optoelectronics
Wuhan 430071 (P. R. China)
and
University of Chinese Academy of Sciences
Beijing 100049 (China)
E-mail: xinzhou@wipm.ac.cn

[+] These authors contributed equally to this work.

results showed that only a para nitro benzoate group modified cyanine probe could serve as a rapid NIR fluorescence-enhanced probe for monitoring and bioimaging of nitroreductase. Duan et al.[13] have developed a cofactor-substrate-based supramolecular luminescent probe for ultra-fast detection of hypoxia-related enzymes in vitro and in vivo by encapsulating a fluorescent substrate L-NO_2 within the NADH mimic-containing metal-organic capsule Zn-MPB. Although significant progress has been made in fluorescent detection of nitroreductase, inherently poor tissue penetration depth limits the scope of application in vivo. Due to the peculiar aggregation-caused quenching effect of the fluorescent probe, the fluorescence intensity can only show a good linear relationship in the relatively low concentration range. The idea of using multimodal imaging in conjugation has gained much attention over the years since it comes to realize the complementary abilities of each one.[14] Ye et al.[15] rationally integrated a fluorogenic reaction into alkaline phosphatase (ALP)-responsive in situ self-assembly to design small-molecule-based activatable NIR fluorescence and magnetic resonance (MR) bimodal probes for molecular imaging. The complex appears suitable for noninvasively measuring and localizing ALP activity in live tumor cells and living mice, with the ability for real-time image-guided resection of liver tumors. Kim et al.[16] reported bimodal contrast agent responds to the Cu^{2+} ion in living cells by enhancing MRI modality signal whereas the optical signal gradually drops. Over the past decade, several researches have focused on designing novel chemical structures to realize multimodal imaging of biomarker of diverse diseases. However, the quantification of certain biomarker over a broad concentration range through imaging methods remain seldom.

Herein, a synergistic combination of tissue depth limit-free ^{19}F MRI with a broad concentration determination range and highly sensitive fluorescence imaging may facilitate the sensitive and selective in vivo imaging of nitroreductase. We propose a dual-mode NIR fluorescence and ^{19}F MRI probe, FCy7-NO_2, by conjugating fluorine and p-nitro groups to the Cy7 for nitroreductase sensing. FCy7-NO_2 showed a sensitive and selective response to overexpressed nitroreductase in hypoxic cells. In vivo hypoxia imaging by FCy7-NO_2 was evaluated on orthotopic lung cancer model mice (Scheme 1). Furthermore, FCy7-NO_2 displayed simultaneous redox behavior whereby nitroreductase-induced nitroxide reduction led to the change in the ^{19}F nuclear magnetic resonance (NMR) chemical shift and fluorescence excitation wavelength. FCy7-NO_2 emerges as a synchronized dual-modality imaging system suitable for molecular imaging of nitroreductase in vivo using both MRI and NIR optical imaging.

Results and Discussion

We selected the Cy7 skeleton as the fluorescent reporting unit to develop the nitroreductase-responsive dual-modal imaging probe FCy7-NO_2. Inspired by a previous nitroreductase-selective fluorescent probe,[17] we modified the indole moieties of Cy7 skeleton with two -NO_2 groups as the nitroreductase recognition units. Meanwhile, two symmetrical fluorines were introduced to the para-position of the -NO_2 groups to facilitate the redox-responsive ^{19}F MRI.

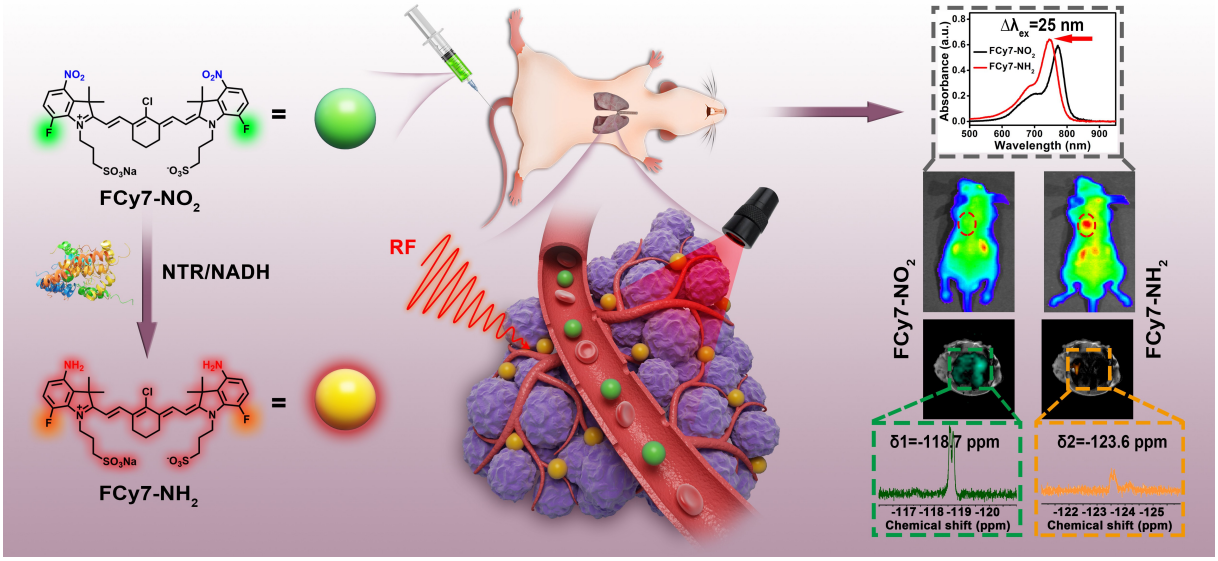

Scheme 1. Schematic illustration of the enzyme-catalyzed mechanism of FCy7-NO_2 for bioimaging of nitroreductase in orthotopic lung cancer model mice by fluorescence imaging and ^{19}F MRI. The probe FCy7-NO_2 was accumulated in the lung area by retrobulbar intravenous injection or pulmonary installation. Then the target probe FCy7-NH_2 was generated by an enzymatic reaction under the action of overexpressed nitroreductase in the orthotopic lung cancer area. Compared with FCy7-NO_2, the fluorescence excitation wavelength of FCy7-NH_2 blue-shifted, and the ^{19}F MR chemical shift changed greatly. We detected FCy7-NH_2 by fluorescence and ^{19}F MRI methods to reflect the overexpression of nitroreductase and then determined the degree of hypoxia in the interior lung so as to reflect the tumor area.

With commercially available 2-fluoro-5-nitroaniline as the starting material, FCy7-NO_2 was conveniently synthesized in five steps, as illustrated in Scheme S1. Notably, the sulfonated form of the probe facilitated its high water solubility and convenient downstream application. The structure of FCy7-NO_2 was confirmed by ^1H, ^{13}C, and ^{19}F NMR, liquid-chromatography mass spectrometry (LC–MS), and high-resolution mass spectrometry (HRMS).

To better understand the molecular recognition between FCy7-NO_2 and nitroreductase, docking calculations were performed for FCy7-NO_2 and Cy7-NO_2 with nitroreductase, respectively (Figure 1A and 1B). Three steps are involved in the nitroreductase-catalyzed reduction reaction, including substrate binding, catalytic reduction, and product departure.[18] Firstly, we investigated the influence of the fluorines on the probe and nitroreductase catalysis. As shown in Figure 1C, the aromatic nitro part of FCy7-NO_2 was more inclined to be close to the catalytic core of nitroreductase compared to Cy7-NO_2 (Figure 1D), which could be driven by the hydrophobic force and the π-π stacking interactions.[19] Subsequently, a transition state was formed by hydrogen bonding between nitroreductase amino acid residues and the nitro groups of FCy7-NO_2. As a result, the FCy7-NO_2 probe formed six hydrogen bonds with amino acid residues Ser18, Arg158, Gly140, Phe138, and Arg178 of nitroreductase (Figure 1E). In contrast, only four hydrogen bonds were observed between Cy7-NO_2 and amino acid residues (Figure 1F). Therefore, the introduction of the two fluorines is accompanied by two additional hydrogen bonds, which promotes the probe to approach the amino acid residues of the nitroreductase hydrophilic part.

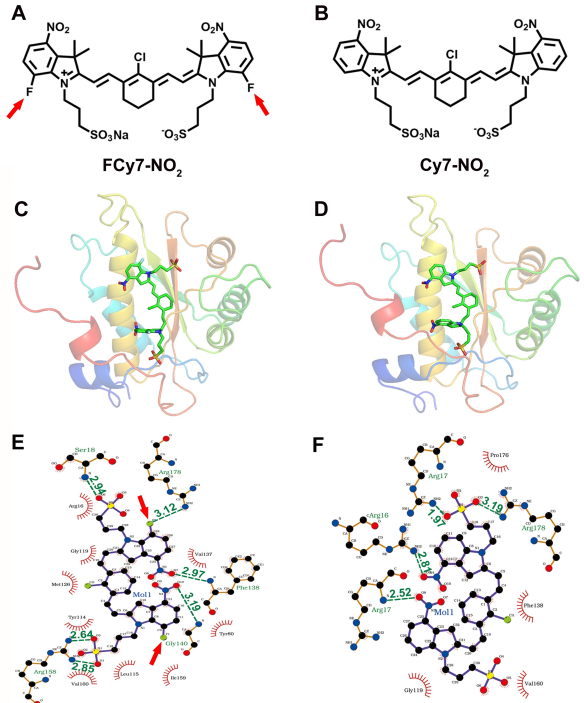

G

Probe 1	FCy7-NO_2	FCy7-NHOH	FCy7-NH_2
Binding energy (kcal mol^{-1})	-8.0	-7.7	-7.6
Probe 2	Cy7-NO_2	Cy7-NHOH	Cy7-NH_2
Binding energy (kcal mol^{-1})	-7.9	-7.8	-7.7

Figure 1. Docking affinity of FCy7-NO_2 and Cy7-NO_2 to nitroreductase. Molecular structure of A) FCy7-NO_2 and B) Cy7-NO_2. Stereoview of probe C) FCy7-NO_2 and D) Cy7-NO_2 binding with nitroreductase. The calculated binding model of E) FCy7-NO_2 and F) Cy7-NO_2 to nitroreductase with the hydrogen bonds indicated as green dashed. G) Calculated binding energies of six molecules with nitroreductase obtained from the molecular docking studies.

The molecular docking calculations also provided the predictive binding energies. The docking affinity was calculated as −7.7 kcal mol^{-1} for amino intermediate, lower than FCy7-NO_2 (−8.0 kcal mol^{-1}) (Figure 1G). A large docking value of FCy7-NO_2 indicated its high binding affinity to nitroreductase, while a low value of intermediates meant that substrates could dissociate from the enzyme easily. Hence the docking calculations explained the outstanding reactivity of the nitroreductase-mediated reduce reaction and suggested that the changes in binding mode and docking affinity were critical for the catalytic reduction reaction process.

To understand the effect of nitroreductase triggered reduction on the photophysical properties of FCy7-NO_2, the UV/Vis absorption and fluorescence emission spectra of the probe were investigated. The probe presented extended adsorption regions from the visible to the NIR region similar to previously studied compounds.[20] The probe initially displayed an absorption peak at 770 nm, along with strong fluorescence emission at 794 nm (Figure S20). The pH had a minimal effect on fluorescence of FCy7-NO_2 and FCy7-NH_2 (Figure S21). It has been demonstrated that the photostability of cyanide fluorescent molecules is usually poor.[21] Two commercially available fluorescent dyes, Cy7 and ICG, have been chosen for comparison. Although the fluorescence intensity of the dyes decreased after both sunlight and UV irradiation for four dyes, the photobleaching resistance of FCy7-NO_2 and FCy7-NH_2 were significantly better than these of Cy7 and ICG. Under sunlight exposure, the fluorescence intensities of ICG and Cy7 decreased to 65 % and 80 %, respectively, on the 7th day, while FCy7-NO_2 and FCy7-NH_2 retained 94 % and 91 % of the initial fluorescence intensity, respectively. The fluorescence intensity of FCy7-NO_2 and FCy7-NH_2 decreased sharply after 5 mins continuous laser irradiation under 500 mW (Figure S22). Presumably, the multiple electron-withdrawing groups (-NO_2 and -F) in FCy7-NO_2 can reduce the electron density of the conjugated π-π structure and thus improve the stability towards photo-oxidation.[22]

The high stability of FCy7-NO_2 and FCy7-NH_2 against oxidative decomposition is beneficial to the nitroreductase reduction study such as long-term storage and exposure to bright light for relatively long periods. Then, the responsive behaviors of FCy7-NO_2 to nitroreductase were investigated by UV/Vis absorption and fluorescence emission spectra. Upon adding an aqueous solution of 0.5 μg mL^{-1} nitroreductase and 10 μM NADH, a significant maximum excitation wavelength blue shift and a fluorescence intensity enhancement were observed for FCy7-NO_2 (Figure 2A and 2B). Consequently, FCy7-NH_2 has been confirmed as the

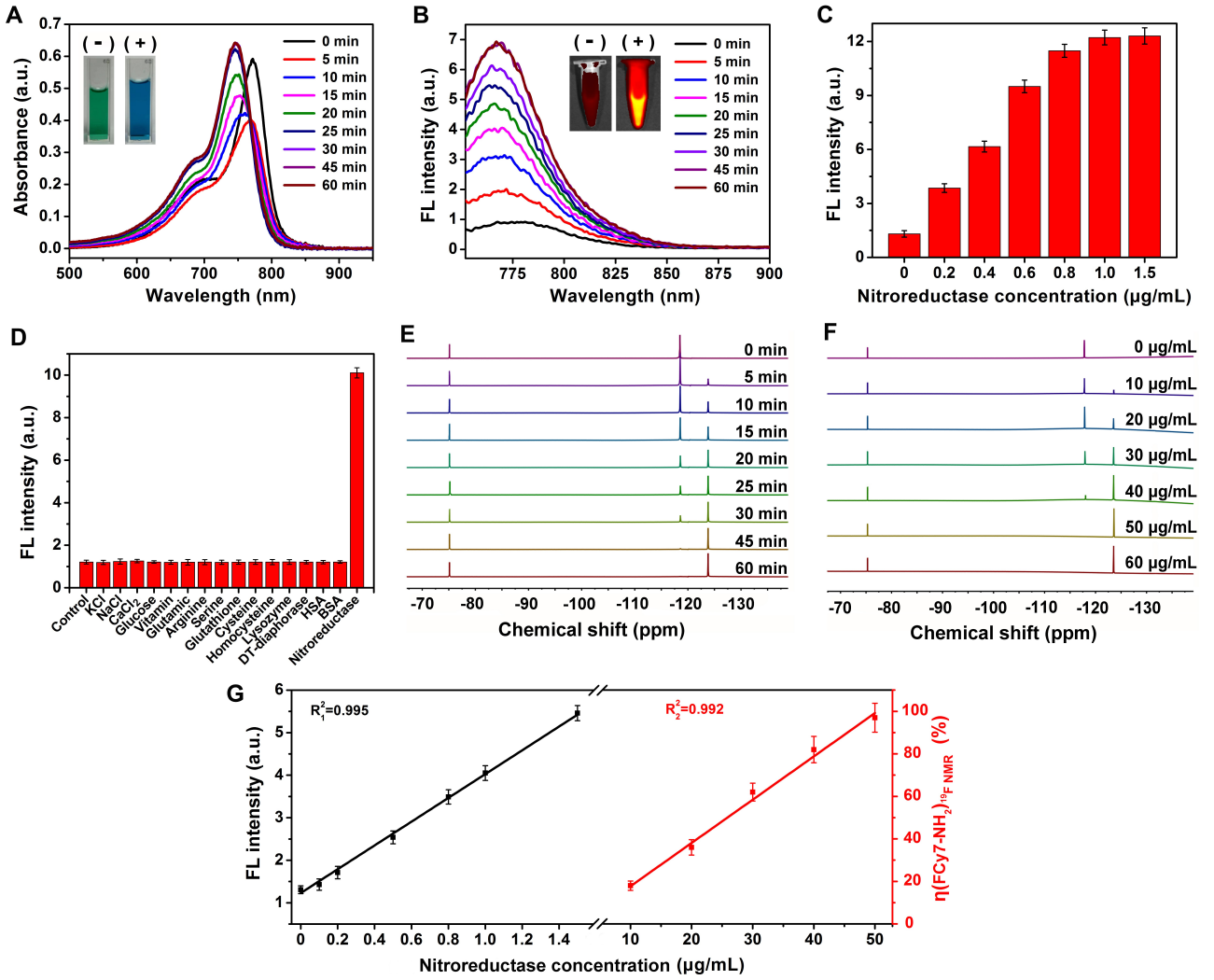

Figure 2. Nitroreductase-responsive optical spectral properties and ^{19}F NMR of FCy7-NO_2. A) UV/Vis absorption and B) fluorescence spectra of FCy7-NO_2 (5 μM) incubated with the nitroreductase for 0–60 min (λ_{ex} = 745 nm, λ_{em} = 773 nm). Inset: photographs (A) and fluorescence images (B) of FCy7-NO_2 pre (-) and post (+) incubation with the nitroreductase (0.5 μg mL^{-1}). C) Fluorescence intensity of FCy7-NO_2 (10 μM) following incubation with varying concentration (0, 0.2, 0.4, 0.6, 0.8, 1.0, and 1.5 μg mL^{-1}, 37 °C) of nitroreductase in the presence of 50 μM NADH for 60 min. D) Fluorescence intensity of FCy7-NO_2 (5 μM) incubated with different kinds of species together with 50 μM NADH in PBS buffer. E) Time-dependent ^{19}F NMR spectra of FCy7-NO_2 (1 mM) after addition of nitroreductase (50 μg mL^{-1}) and NADH (5 mM) at 37 °C in PBS. F) Concentration-dependent ^{19}F NMR spectra of FCy7-NO_2 (1 mM) after incubation with varying concentration (0, 10, 20, 30, 40, 50 and 60 μg mL^{-1}) of nitroreductase for 60 min. CF_3COONa (−75.3 ppm) was used as the ^{19}F NMR reference. G) Nitroreductase concentration-dependent fluorescence intensity (black) at low nitroreductase concentration (≤1.5 μg mL^{-1}) and nitroreductase concentration-dependent ^{19}F NMR (red) at high nitroreductase concentration (10–50 μg mL^{-1}), respectively. The black and red lines represent the linear fitting of the data.

product by NMR and HRMS (Figure S23–S26). Furthermore, it could be observed from the UV/Vis experiment that the maximum UV absorption of the solution decreased sharply at the first time point (5 min) of the reaction and then increased gradually until reaching a plateau in about 1 hour, accompanied by the blue shift of the maximum absorption peak. Finally, the maximum UV/Vis absorption of the solution was blue-shifted from 770 nm to 745 nm. Apparently, converting the -NO_2 groups to the -NH_2 groups was a multi-step process involving several intermediates.[23] The steep drop of the maximum UV absorption at 5 min also indicated the interactions between the -NO_2 groups and nitroreductase, which initiated the downstream transformations.

The fluorescence emission spectra also reflected the corresponding variation tendency. The maximum UV/Vis absorption of the target product FCy7-NH_2 was at 745 nm, which was used as the excitation wavelength to monitor the formation of FCy7-NH_2 using the fluorescence intensity of the incubated solution. As the incubation time increased, FCy7-NO_2 gradually transformed into FCy7-NH_2, accompanied by a progressive enhancement in the fluorescence intensity until a maximum emission reached about 1 hour. Even though the UV/Vis absorption of the substrate FCy7-NO_2 and the product FCy7-NH_2 overlaps at 745 nm, the

fluorescence of the solution was still strong at the beginning state, and the overall fluorescence intensity of the solution was increased by 7 times after 1-hour incubation.

To further study the effect of nitroreductase concentration on the fluorescence property of FCy7-NO_2, different concentrations of nitroreductase with five equivalents of NADH were added to the solution of FCy7-NO_2 to monitor the reaction process. Notably, about 1 $\mu g\,mL^{-1}$ of enzyme can completely transfer FCy7-NO_2 into FCy7-NH_2 (Figure 2C). Owing to its high reactivity towards nitroreductase, FCy7-NO_2 exhibited a prominent selectivity for nitroreductase over an array of potentially competitive reduction agents (Figure 2D). Even at a super low concentration beyond its physiological range in tumor tissues, nitroreductase still gave a significant response in fluorescence (Figure 2G and S27).

In addition to the highly sensitive fluorescence method to detect nitroreductase, incorporation of ^{19}F into the Cy7 skeleton was allowed for nitroreductase detection by ^{19}F NMR. As the high signal intensity is beneficial for monitoring a reaction with ^{19}F NMR, we first investigated the chemical shift changes ($\Delta\delta$) of a 1-fluoro-4-nitrobenzene and 1-trifluoromethyl-4-nitrobenzene during the enzymatic reaction. As the fluorine atom was directly connected to the benzene ring in 1-fluoro-4-nitrobenzene, reducing the electron-withdrawn nitro group to the electron-donating amino group significantly improved the electron density of the fluorine, which led to a chemical shift change of 24.8 ppm. In contrast, the electron density improvement on fluorine atoms was severely weakened by the carbon-carbon single bond between the benzene group and the trifluoromethyl group in 1-trifluoromethyl-4-nitrobenzene, which led to a much smaller chemical shift change of 2.0 ppm (Figure S28). Therefore, we selected 1-fluoro-4-nitrobenzene as the key structure with large chemical shift changes to monitor nitroreductase. In the nitroreductase concentration-dependent ^{19}F NMR, the ^{19}F peak of FCy7-NO_2 at −118.6 ppm was gradually replaced by the ^{19}F peak of FCy7-NH_2 at −123.8 ppm with the increasing of nitroreductase in the system. The ^{19}F peak of FCy7-NO_2 completely disappeared after 1 hour of incubation (Figure 2E). This trend is in good agreement with the optical spectroscopic results, which also confirms the feasibility of using ^{19}F NMR to detect and quantify nitroreductase, especially in the high concentration range (Figure 2F, 2G, and S29). Furthermore, dicoumarin, a nitroreductase inhibitor, was employed to probe the reaction (Figure S30). It was found that about 40 μM dicoumarin inhibited entirely the reduction of FCy7-NO_2 by nitroreductase at 50 $\mu g\,mL^{-1}$, which showed that the ^{19}F NMR signal change was solely caused by the nitroreductase catalyzed reduction.

We next employed FCy7-NO_2 to detect the nitroreductase levels in living cells using confocal microscopy to monitor the nitroreductase-dependent fluorescence signal intensity. Before applying FCy7-NO_2 to detect nitroreductase activity in living cells, we evaluated its cytotoxicity against human alveolar basal epithelial cells (A549) using the standard MTT cytotoxicity assay (Figure S31). In the presence of FCy7-NO_2 at 5–50 μM, the cellular viabilities were estimated to be higher than 80 % after incubation for 24 h, demonstrating FCy7-NO_2 as a biocompatible probe for cell studies.

We then applied FCy7-NO_2 to detect nitroreductase activity in living A549 cells, which have been reported to overexpress nitroreductase under hypoxic conditions.[24] The A549 cells were grown under normoxic conditions (20 % O_2) and different hypoxic conditions (10 %, 5 %, and 1 % O_2) for 6 hours and then treated with 10 μM FCy7-NO_2 for 4 hours. It was observed that the A549 cells incubated under normoxic conditions showed a weak NIR fluorescence signal relatively. As expected, the cells cultured under decreased oxygen concentrations showed increased fluorescence intensity in the NIR region, indicating that these cells can express nitroreductase to trigger the reaction (Figure 3A). More hypoxia conditions (1 % O_2) resulted in higher fluorescence signal intensity, which was 6.5 times higher than that of normoxic conditions (Figure S32). Accordingly, the phenomenon can be ascribed to the nitroreductase-catalyzed reduction of FCy7-NO_2 into FCy7-NH_2, giving the increased fluorescence intensities under the excitation wavelength of 745 nm. The competitive reaction of nitroreductase was also carried out using the nitroreductase inhibitor dicoumarin. With the increase of dicoumarin concentration, the intensity of intracellular fluorescence decreased, indicating that the nitroreductase-catalyzed reduction of FCy7-NO_2 was inhibited by dicoumarin (Figure 3B and S33).

We next employed ^{19}F MRI to monitor the in vitro transformation of FCy7-NO_2 by nitroreductase. To identify the optimal FCy7-NO_2 concentration for ^{19}F MRI, a ^{19}F MRI phantom experiment was carried out with a series of FCy7-NO_2 solutions in PBS. It was found that FCy7-NO_2 at 10 mM presented the strongest ^{19}F signal intensity and the signal intensity decreased when further increased concentration (Figure S34). Presumably, a high concentration of FCy7-NO_2 leads to its severe aggregation and reduces the ^{19}F signal intensity. Then, different amounts of nitroreductase were loaded into a 1 mM FCy7-NO_2 solution, respectively (Figure S35). The ^{19}F MR images showed the ^{19}F intensity improvement of FCy7-NH_2 and the ^{19}F intensity reduction of FCy7-NO_2 with the increase of nitroreductase amount, which illustrated the feasibility of using FCy7-NO_2 to detect nitroreductase in biological settings.

To showcase the utility of FCy7-NO_2 for biological nitroreductase imaging, we employed this reagent to observe intracellular nitroreductase expression in A549 cells with ^{19}F MRI. We performed two separate experiments for nitroreductase detection based on ^{19}F MRI. First, A549 cells were cultured under hypoxia (1 % O_2) for 4 hours and then transferred to normal oxygen for culture. After adding 0.5 mM FCy7-NO_2 and incubating for 12 h, the cells were lysed and mixed with the culture medium for ^{19}F MRI. As a result, the ^{19}F MRI signal of FCy7-NH_2 at −123.8 ppm can be detected, and we can calculate how much nitroreductase was in the cell lysate based on the comparison of its signal intensity with that of the reference (Figure S36). The concentration of nitroreductase after cell lysis was determined as 13.6 $\mu g\,mL^{-1}$, which can not be quantified using the fluorescence method. However, the concentration was fall-

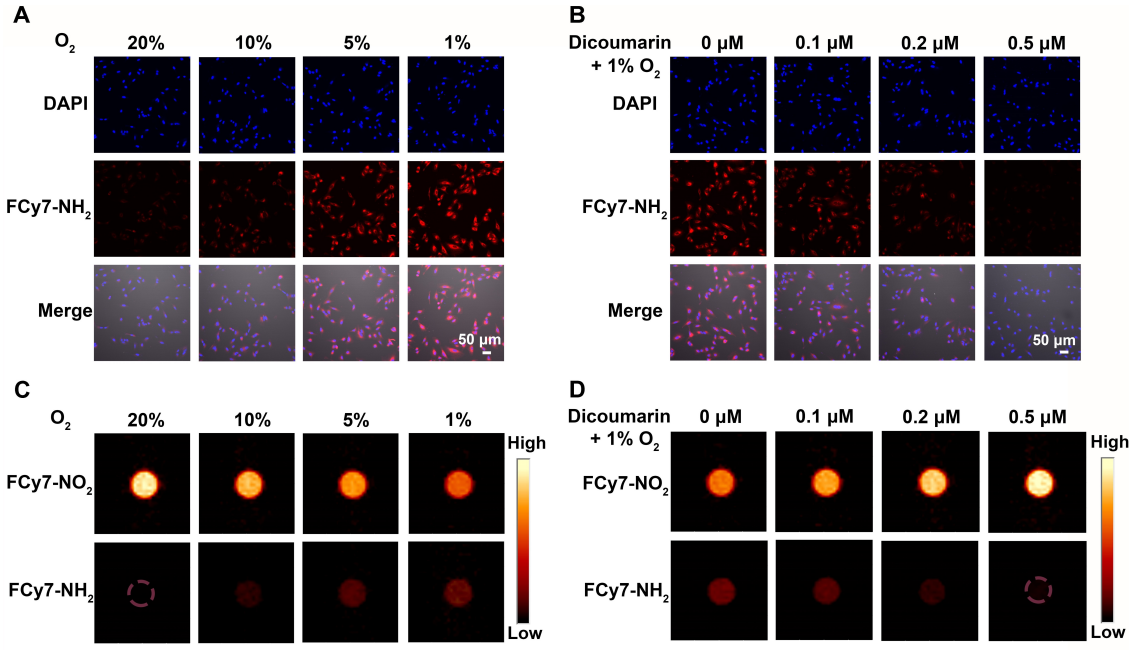

Figure 3. Imaging of FCy7-NO_2 activity in living tumor cells. Confocal fluorescence microscopy imaging of A549 cells incubated with FCy7-NO_2 (10 μM) under A) different oxygen concentration conditions (20%, 10%, 5% and 1%) and B) different dicoumarin concentration conditions (0, 0.1, 0.2 and 0.5 μM). The fluorescence images were collected at the NIR channel (800 ± 30 nm, λ_{ex} = 745 nm CW laser). Scale bar = 50 μm. ^{19}F MR phantom images of A549 cells incubated with FCy7-NO_2 (0.5 mM) under C) different oxygen concentration conditions (20%, 10%, 5% and 1%) and D) different dicoumarin concentration conditions (0, 0.1, 0.2 and 0.5 μM), respectively.

ing into the ^{19}F detection range. Therefore, we can calculate the corresponding nitroreductase content according to the ^{19}F MRI signals of FCy7-NH_2 in the A549 cell lysate. Second, A549 cells were cultured under different hypoxic conditions for 4 h or different incubation times under 1% O_2 condition and then transferred to normal oxygen for culture. After adding the same concentration of FCy7-NO_2 (0.5 mM) and incubating for 12 hours, the cells were lysed and mixed with the culture medium for ^{19}F MRI/NMR (Figure 3C and S37). The signal of FCy7-NH_2 became stronger as the oxygen of the cell culture decreased or the incubation time in the hypoxia was prolonged. The above experiments confirmed that the more hypoxia and the longer the incubation time will produce more nitroreductase in A549 cells.

The strong ^{19}F signal of FCy7-NH_2 in ^{19}F MRI showed the expression of nitroreductase in A549 cells under hypoxic conditions. We can also quantify the different nitroreductase contents in the A549 cells according to the signal ratio of FCy7-NH_2 and FCy7-NO_2 (Figure S38). Additionally, the concentration of nitroreductase was proportional to the fraction of FCy7-NH_2 determined from NMR even in a higher concentration range. This enabled the concentration of nitroreductase to be quantified using MRI, which is critical for diagnosing the stage of the tumor. The experiments of dicoumarin as an inhibitor of nitroreductase enzyme activity were also tested by ^{19}F MRI in A549 cells, consistent with the results of cell confocal experiments (Figure 3D).

To elucidate the ability of FCy7-NO_2 for in vivo imaging, nitroreductase-triggered activation of NIR-fluorescence and MR contrast were investigated in living mice. Initial studies used left lung cancer model mice with a healthy right lung for comparison, where nitroreductase expression was driven by the size of the tumor, thus presenting inside the diseased lung. Injection of mice with and without FCy7-NO_2 resulted in notable differences in fluorescence signal intensities. We then monitored the flux of the probe over a long period. Intriguingly, the probe tended to flow to the tumor and kidney area in the first 4 hours, which showed lower fluorescence intensity that possibly belonged to the presence of the large amount of FCy7-NO_2. With time increased, the lung and kidney signal intensity has increased and decreased, respectively (Figure 4A and 4B), suggesting that more FCy7-NO_2 has been transformed into FCy7-NH_2 to trigger the higher fluorescence intensity. At the 24-hour time point, the fluorescence intensity in the left lung tumor area reached a maximum. It was most strongly contrasted with the surrounding fluorescence, 9.2 times that of the surrounding average fluorescence intensity. Fluorescence contrast was observed in the left lung region until the 72-hour time point. Then, the biodistribution of FCy7-NO_2 was examined via ex vivo fluorescence imaging of the main organs. The average fluorescence intensity of the left lung was 2.9 times that of the kidney and 7.4 times that of the liver, respectively (Figure 4C, 4D and S39). The results demonstrated that the reduction reaction of nitroreductase mostly happened in the left cancerous lung. This experiment fully proved the feasibility of using this probe to detect

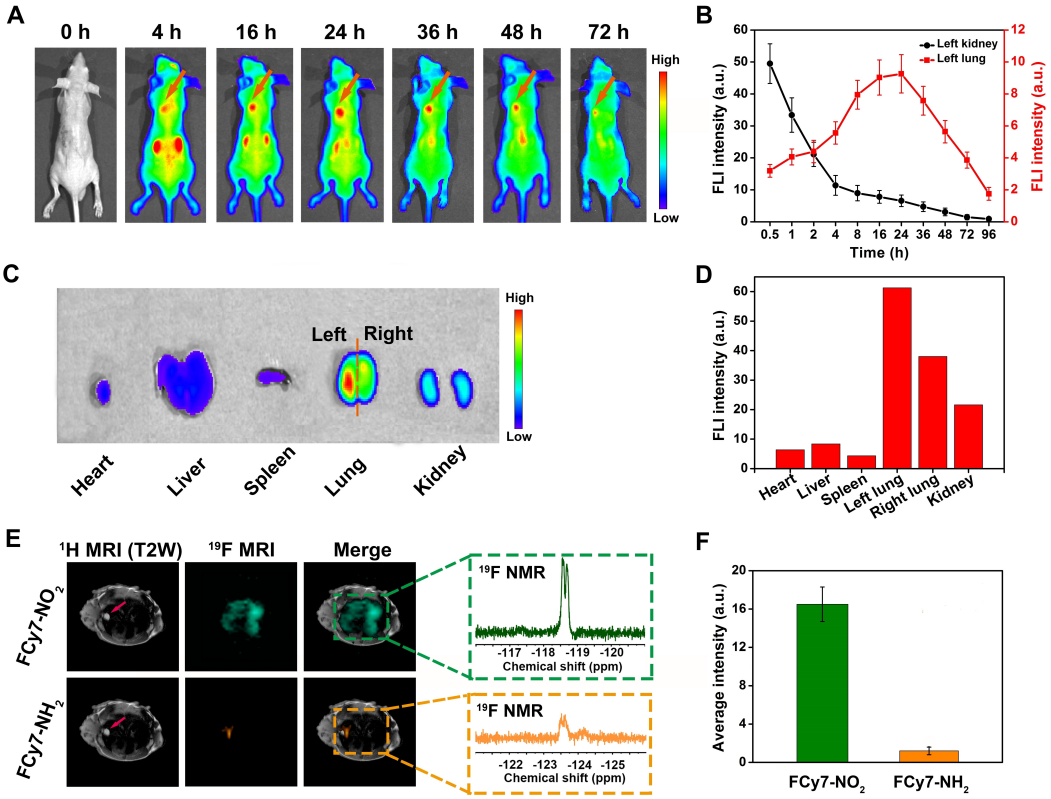

Figure 4. FCy7-NO_2 was used to identify orthotopic lung cancer by in vivo NIR fluorescence and ^{19}F MR imaging. A) Time-based in vivo fluorescence imaging of orthotopic lung cancer model mouse after injecting FCy7-NO_2 (100 μM, 100 μL) via posterior venous plexus injection. The orange arrow indicates the location of lung cancer. B) The fluorescence intensity of FCy7-NH_2 in the left lung (red) and left kidney (black) as a function of time (0.5–96 h). C) Fluorescence imaging and D) fluorescence intensity measurements of isolated organs at 24 h post-injection of the probe. E) In vivo ^{19}F MRI of an orthotopic lung cancer model mouse after drip irrigation of FCy7-NO_2 (20 μL, 10 mM, normal saline including 2% DMSO as solution). The contents of the substrate (FCy7-NO_2) and target product (FCy7-NH_2) were detected at −118.7 ppm and −123.6 ppm, respectively. ^{1}H MRI was tested by T2 weighted image (T2WI), and ^{19}F MRI was tested by density weighted image. F) ^{19}F MRI intensity of FCy7-NO_2 and FCy7-NH_2 in the lung area.

orthotopic lung cancer. The H&E staining also confirmed the formation of the left lung tumor in situ (Figure S40).

In orthotopic lung cancer model mice, a 20 μL 10 mM contrast medium was injected into the lung area by drip irrigation.[25] After 2 hours, we can detect the existence of FCy7-NO_2 both in the left lung and the right lung. In other words, the signal of the ^{19}F MRI of FCy7-NO_2 filled the entire lung without any difference. With the diffusion of the contrast agent in the tumor area and the prolongation of the enzymatic action, the increased ^{19}F signal belonged to FCy7-NH_2 was detected at −123.6 ppm in the left lung tumor area, indicating that FCy7-NO_2 could monitor the alterations of nitroreductase in living animals by the chemical shift imaging method (Figure 4E and 4F). Even though very few FCy7-NO_2 have been catalytically transformed into FCy7-NH_2 due to the small amount of nitroreductase present in the tumor area, the signal of ^{19}F was high enough to be achieved. Taken together, this result confirmed that ^{19}F MRI could be used to detect the presence of nitroreductase in vivo.

Conclusion

In summary, we have developed a small-molecular-based activable NIR fluorescence/MRI bimodal probe for real-time in vivo imaging of nitroreductase activity. The enzyme-triggered reactions were validated through a series of in vitro and in vivo experiments. Given simultaneous enhancement in NIR fluorescence and upshift of the ^{19}F signal by NMR, FCy7-NO_2 appeared suitable for non-invasively measuring nitroreductase overexpressed in lung cancer cells and model mice. Specifically, by combining the ^{19}F NMR and fluorescence methods, the concentration of the nitroreductase can be quantified in a broad concentration range, which is far superior to the single imaging method. Therefore, we can accurately map the nitroreductase in a specific region, distinguish the boundary between normal and hypoxic tissues according to the level of nitroreductase content, and quantitatively assess the degree of hypoxia, providing clinicians with a favorable tool for evaluating the disease. This work also demonstrated that incorporating multiple stimuli-responsiveness into multimodal probes would inspire new interest in designing intelligent

probes for other biochemical processes, including other enzymatic activities, small molecules, and metal ions.

Acknowledgements

This work is supported by the Key Technology Research and Development Program (2018YFA0704000) and the National Natural Science Foundation of China (91859206, 21874150, U21A20392, 82127802, 21921004). Xin Zhou acknowledges the support from the Tencent Foundation through the XPLORER PRIZE.

Conflict of Interest

The authors declare no conflict of interest.

Data Availability Statement

The data that support the findings of this study are available from the corresponding author upon reasonable request.

Keywords: ^{19}F MRI · Biosensors · Fluorescence Imaging · Hypoxia · Nitroreductase

[1] H. Sung, J. Ferlay, R. L. Siegel, M. Laversanne, I. Soerjomataram, A. Jemal, F. Bray, *Ca-Cancer J. Clin.* **2021**, *71*, 209–249.

[2] a) H. J. de Koning, C. M. van der Aalst, P. A. de Jong, E. T. Scholten, K. Nackaerts, M. A. Heuvelmans, J.-W. J. Lammers, C. Weenink, U. Yousaf-Khan, N. Horeweg, S. van 't Westeinde, M. Prokop, W. P. Mali, F. A. A. Mohamed Hoesein, P. M. A. van Ooijen, J. G. J. V. Aerts, M. A. den Bakker, E. Thunnissen, J. Verschakelen, R. Vliegenthart, J. E. Walter, K. ten Haaf, H. J. M. Groen, M. Oudkerk, *N. Engl. J. Med.* **2020**, *382*, 503–513; b) D. R. Aberle, A. M. Adams, C. D. Berg, W. C. Black, J. D. Clapp, R. M. Fagerstrom, I. F. Gareen, C. Gatsonis, P. M. Marcus, J. D. Sicks, *N. Engl. J. Med.* **2011**, *365*, 395–409.

[3] a) G. B. Frisoni, N. C. Fox, C. R. Jack, P. Scheltens, P. M. Thompson, *Nat. Rev. Neurol.* **2010**, *6*, 67–77; b) J. P. B. O'Connor, A. Jackson, G. J. M. Parker, C. Roberts, G. C. Jayson, *Nat. Rev. Clin. Oncol.* **2012**, *9*, 167–177; c) J. Lu, J. Sun, F. Li, J. Wang, J. Liu, D. Kim, C. Fan, T. Hyeon, D. Ling, *J. Am. Chem. Soc.* **2018**, *140*, 10071–10074; d) L. Wang, Z. Wang, X. Li, Y. Zhang, M. Yin, J. Li, H. Song, J. Shi, D. Ling, L. Wang, N. Chen, C. Fan, *Nano Res.* **2018**, *11*, 2746–2755.

[4] A. S. Khan, R. L. Harvey, J. R. Birchall, R. K. Irwin, P. Nikolaou, G. Schrank, K. Emami, A. Dummer, M. J. Barlow, B. M. Goodson, E. Y. Chekmenev, *Angew. Chem. Int. Ed.* **2021**, *60*, 22126–22147; *Angew. Chem.* **2021**, *133*, 22298–22319.

[5] a) R. Shusterman-Krush, N. D. Tirukoti, A. K. Bandela, L. Avram, H. Allouche-Arnon, X. Cai, B. C. Gibb, A. Bar-Shir, *Angew. Chem. Int. Ed.* **2021**, *60*, 15405–15411; *Angew. Chem.* **2021**, *133*, 15533–15539; b) K. Akazawa, F. Sugihara, T. Nakamura, H. Matsushita, H. Mukai, R. Akimoto, M. Minoshima, S. Mizukami, K. Kikuchi, *Angew. Chem. Int. Ed.* **2018**, *57*, 16742–16747; *Angew. Chem.* **2018**, *130*, 16984–16989.

[6] a) J. M. Brown, W. R. Wilson, *Nat. Rev. Cancer* **2004**, *4*, 437–447; b) W. R. Wilson, M. P. Hay, *Nat. Rev. Cancer* **2011**, *11*, 393–410.

[7] I. Dagogo-Jack, A. T. Shaw, *Nat. Rev. Clin. Oncol.* **2018**, *15*, 81–94.

[8] a) Y. Ye, Q. Hu, H. Chen, K. Liang, Y. Yuan, Y. Xiang, H. Ruan, Z. Zhang, A. Song, H. Zhang, L. Liu, L. Diao, Y. Lou, B. Zhou, L. Wang, S. Zhou, J. Gao, E. Jonasch, S. H. Lin, Y. Xia, C. Lin, L. Yang, G. B. Mills, H. Liang, L. Han, *Nat. Metab.* **2019**, *1*, 431–444; b) C.-C. Huang, W.-T. Chia, M.-F. Chung, K.-J. Lin, C.-W. Hsiao, C. Jin, W.-H. Lim, C.-C. Chen, H.-W. Sung, *J. Am. Chem. Soc.* **2016**, *138*, 5222–5225; c) S. Kuang, L. Sun, X. Zhang, X. Liao, T. W. Rees, L. Zeng, Y. Chen, X. Zhang, L. Ji, H. Chao, *Angew. Chem. Int. Ed.* **2020**, *59*, 20697–20703; *Angew. Chem.* **2020**, *132*, 20878–20884.

[9] a) C. Huang, W. Tan, J. Zheng, C. Zhu, J. Huo, R. Yang, *ACS Appl. Mater. Interfaces* **2019**, *11*, 25740–25749; b) S. Danson, T. H. Ward, J. Butler, M. Ranson, *Cancer Treat. Rev.* **2004**, *30*, 437–449; c) Y. Zhang, W. Zhao, Y. Chen, H. Yuan, H. Fang, S. Yao, C. Zhang, H. Xu, N. Li, Z. Liu, Z. Guo, Q. Zhao, Y. Liang, W. He, *Nat. Commun.* **2021**, *12*, 2772; d) S. He, J. Li, Y. Lyu, J. Huang, K. Pu, *J. Am. Chem. Soc.* **2020**, *142*, 7075–7082; e) W.-C. Geng, S. Jia, Z. Zheng, Z. Li, D. Ding, D.-S. Guo, *Angew. Chem. Int. Ed.* **2019**, *58*, 2377–2381; *Angew. Chem.* **2019**, *131*, 2399–2403; f) L. Sun, Y. Gao, Y. Xu, J. Chao, H. Liu, L. Wang, D. Li, C. Fan, *J. Am. Chem. Soc.* **2017**, *139*, 17525–17532; g) F. Wang, Y. Zhu, L. Zhou, L. Pan, Z. Cui, Q. Fei, S. Luo, D. Pan, Q. Huang, R. Wang, C. Zhao, H. Tian, C. Fan, *Angew. Chem. Int. Ed.* **2015**, *54*, 7349–7353; *Angew. Chem.* **2015**, *127*, 7457–7461; h) J. Huang, X. Chen, Y. Jiang, C. Zhang, S. He, H. Wang, K. Pu, *Nat. Mater.* **2022**, *21*, 598–607.

[10] a) S. Curado, D. Y. R. Stainier, R. M. Anderson, *Nat. Protoc.* **2008**, *3*, 948–954; b) Y. Liu, L. Teng, L. Chen, H. Ma, H.-W. Liu, X.-B. Zhang, *Chem. Sci.* **2018**, *9*, 5347–5353; c) H. J. Knox, J. Hedhli, T. W. Kim, K. Khalili, L. W. Dobrucki, J. Chan, *Nat. Commun.* **2017**, *8*, 1794; d) B. Brennecke, Q. Wang, Q. Zhang, H.-Y. Hu, M. Nazaré, *Angew. Chem. Int. Ed.* **2020**, *59*, 8512–8516; *Angew. Chem.* **2020**, *132*, 8590–8594.

[11] Z. Thiel, P. Rivera-Fuentes, *Angew. Chem. Int. Ed.* **2019**, *58*, 11474–11478; *Angew. Chem.* **2019**, *131*, 11597–11602.

[12] Y. Li, Y. Sun, J. Li, Q. Su, W. Yuan, Y. Dai, C. Han, Q. Wang, W. Feng, F. Li, *J. Am. Chem. Soc.* **2015**, *137*, 6407–6416.

[13] Y. Jiao, L. Zhang, X. Gao, W. Si, C. Duan, *Angew. Chem. Int. Ed.* **2020**, *59*, 6021–6027; *Angew. Chem.* **2020**, *132*, 6077–6083.

[14] A. Louie, *Chem. Rev.* **2010**, *110*, 3146–3195.

[15] R. Yan, Y. Hu, F. Liu, S. Wei, D. Fang, A. J. Shuhendler, H. Liu, H.-Y. Chen, D. Ye, *J. Am. Chem. Soc.* **2019**, *141*, 10331–10341.

[16] J. H. Jang, S. Bhuniya, J. Kang, A. Yeom, K. S. Hong, J. S. Kim, *Org. Lett.* **2013**, *15*, 4702–4705.

[17] a) J. Ouyang, L. Sun, Z. Zeng, C. Zeng, F. Zeng, S. Wu, *Angew. Chem. Int. Ed.* **2020**, *59*, 10111–10121; *Angew. Chem.* **2020**, *132*, 10197–10207; b) A. Chevalier, Y. Zhang, O. M. Khdour, J. B. Kaye, S. M. Hecht, *J. Am. Chem. Soc.* **2016**, *138*, 12009–12012.

[18] D. Cui, J. Huang, X. Zhen, J. Li, Y. Jiang, K. Pu, *Angew. Chem. Int. Ed.* **2019**, *58*, 5920–5924; *Angew. Chem.* **2019**, *131*, 5981–5985.

[19] A. Dougherty Dennis, *Science* **1996**, *271*, 163–168.

[20] a) J. Yin, Y. Kwon, D. Kim, D. Lee, G. Kim, Y. Hu, J.-H. Ryu, J. Yoon, *Nat. Protoc.* **2015**, *10*, 1742–1754; b) Z. Zeng, S. S. Liew, X. Wei, K. Pu, *Angew. Chem. Int. Ed.* **2021**, *60*, 26454–26475; *Angew. Chem.* **2021**, *133*, 26658–26679.

[21] R. B. Altman, D. S. Terry, Z. Zhou, Q. Zheng, P. Geggier, R. A. Kolster, Y. Zhao, J. A. Javitch, J. D. Warren, S. C. Blanchard, *Nat. Methods* **2012**, *9*, 68–71.

[22] a) W. Wang, J. J. Han, L.-Q. Wang, L.-S. Li, W. J. Shaw, A. D. Q. Li, *Nano Lett.* **2003**, *3*, 455–458; b) M. O. Sinnokrot, C. D. Sherrill, *J. Am. Chem. Soc.* **2004**, *126*, 7690–7697.

[23] a) H. Abdullah, N. S. Gultom, H. Shuwanto, W. L. Kebede, D.-H. Kuo, *ACS Appl. Mater. Interfaces* **2020**, *12*, 43761–43770; b) W. Eck, V. Stadler, W. Geyer, M. Zharnikov, A. Gölzhäuser, M. Grunze, *Adv. Mater.* **2000**, *12*, 805–808; c) B. Shi, N. Ren, L. Gu, G. Xu, R. Wang, T. Zhu, Y. Zhu, C. Fan, C. Zhao, H. Tian, *Angew. Chem. Int. Ed.* **2019**, *58*, 16826–16830; *Angew. Chem.* **2019**, *131*, 16982–16986.

[24] R. Wang, J. Chen, J. Gao, J.-A. Chen, G. Xu, T. Zhu, X. Gu, Z. Guo, W.-H. Zhu, C. Zhao, *Chem. Sci.* **2019**, *10*, 7222–7227.

[25] M. Zhang, H. Li, H. Li, X. Zhao, Q. Zhou, Q. Rao, Y. Han, Y. Lan, H. Deng, X. Sun, X. Lou, C. Ye, X. Zhou, *Magn. Reson. Med.* **2020**, *84*, 569–578.

Manuscript received: September 13, 2022
Accepted manuscript online: October 20, 2022
Version of record online: November 17, 2022